Chapter 3

PINOID plasma membrane association and calmodulin binding converge on an amphipathic alpha helix/IQ-like motif

Yuanwei Fan, Eike.H.Rademacher[1], Elco Backus[2], Martinus Schneijderberg, Ser van der Burght, Remko Offringa

Molecular and Developmental Genetics, Institute Biology Leiden, Leiden University, Sylviusweg 72, 2333 BE Leiden, The Netherlands

[1] Current affiliation: Rijk Zwaan Breeding B.V., Burgemeester Crezélaan 40, 2678 ZG De Lier, The Netherlands

[2] Current affiliation: Crucell, P.O.Box 248, 2301CA Leiden, The Netherlands

Summary

The *Arabidopsis* AGC protein kinase PINOID (PID) is a key regulator of plant adaptive responses to environmental signals. PID determines the direction of polar transport of the plant hormone auxin, a central regulator of plant development and growth, by directing the asymmetric subcellular distribution of PIN proteins through phosphorylation of these auxin efflux carriers. By affecting the activity of the PID protein kinase, environmental signals can change the polarity of auxin transport, and thereby the direction of plant growth. In chapter 2 we showed that PID kinase activity is repressed through Ca^{2+}-dependent binding of the calmodulin-like protein CML12/TCH3/, which sequesters PID from the plasma membrane (PM) to the cytosol, away from its PIN phosphorylation targets. Here we show that CML10 and the calmodulin CAM2, two proteins closely related to TCH3, are also able to recruit PID from the PM. In view of the redundant role of the calmodulins (CaMs) and CMLs in regulating PID activity , we fine-mapped the PM associated domain and the CML/CaM binding domain in PID with the final aim to identify amino acid substitutions that would allow to functionally analyse the role of CML/CaM recruitment throughout plant development. Our analysis revealed that PID CML/CaM binding and PM association sites converge on an amphipathic alpha helix/IQ-like motif in the PID insertion domain, and that the two functionalities cannot be separated. This dual interaction domain allows an elegant novel mechanism of protein kinase activity regulation, by which cytosolic Ca^{2+} concentrations determine whether the kinase is available to phosphorylate substrate proteins.

Introduction

As sessile organisms, plants continuously monitor their environment in order to accurately respond to changes with adaptive growth or defense mechanisms. To do this, plants have acquired a complex network of signal perception and -transduction systems, where cross talk between signaling pathways is for an important part mediated by plant hormones. The central regulator in plant adaptive development and growth is the plant hormone auxin, or indole-3-acetic acid (IAA), that orchestrates growth and positions of new organ initiation sites through local biosynthesis- and polar transport-generated maxima and minima (Tanaka et al., 2006).

PIN auxin efflux carriers have been identified as important drivers of polar auxin transport, as they determine the direction of this cell-to-cell transport through their asymmetric subcellular localization (Petrasek et al., 2006; Wisniewska et al., 2006). PIN polar localization is responsive to internal and external signals, and is regulated by post-translational modification, such as phosphorylation and ubiquitination, leading to changes in PIN trafficking and turn over (Geldner et al., 2001; Friml et al., 2004; Abas et al., 2006; Sauer et al., 2006). The AGC protein serine/threonine kinase PINOID (PID), and its close homologs WAG1 and WAG2 are key determinants in the polar localization of PIN proteins, as they can cause transcytosis-mediated switches in PIN polarity by phosphorylating PIN proteins in their central hydrophilic loop (Friml et al., 2004; Dhonukshe et al., 2010; Huang et al., 2010). One way for environmental signals to regulate endogenous auxin levels would be by regulating the activity of the AGC3 kinases and thereby altering the direction of auxin transport. In fact, light was shown to down-regulate *PID* gene expression and this has been proposed to redirect PIN3 polarity in hypocotyl endodermis cells during the phototropic response in *Arabidopsis* seedlings (Ding et al., 2011). In Chapter 2 of this thesis we showed that elevated auxin levels induced Ca^{2+}-dependent sequestration of PID by the calmodulin-like protein TCH3 from the PM to the cytosol, and that this leads to PIN2 depolarization, which is needed to maximize the gravitropic response of *Arabidopsis* roots. Interestingly, both auxin and mechanical stress induce elevation of Ca^{2+} levels (Monshausen et al., 2009; Monshausen et al., 2011), making it likely that the PID-TCH3 signaling complex also acts in regulating PIN polarity in response to mechanical signals.

There are seven almost identical CaMs in *Arabidopsis* and 50 CaM-like proteins (CMLs). The CMLs are predicted to be the potential Ca^{2+} sensors and share at least 16% amino acid identity with CaMs. The members of the CaM/CML family are separated into nine groups based on amino acid sequence divergence (McCormack et al., 2005).

CaMs use a linker domain to connect two pairs of Ca^{2+} binding pockets called 'EF hands'. EF hands have micromolar affinity with Ca^{2+} and upon Ca^{2+} binding their conformation is changed. TCH3 is closely related to CaM, but has six EF hands instead of the four EF hands in CaMs or CMLs, because of an exact duplication of EF hands 1 and 2 in the N-terminus of the protein (McCormack et al., 2005).

Previous analysis showed that *tch3* loss-of-function mutants only show mild phenotypes, such as a slight delay in root gravitropism (Chapter 2), suggesting that other members of the CaM/CML protein family act redundantly with TCH3. Here we show that, indeed, CML10, CAM2, and most likely also the other 6 CAMs are able to interact with PID and to sequester PID from the PM. As this complicated investigating the role of the PID-CML signaling complex by looking at the function of the CaM/CMLs in plant development, we decided to map the PM association and CaM binding domains in PID, with the objective to generate a fully functional mutant PID protein, except for its interaction with the CaM/CMLs (untouchable PID).

One characteristic of PID and the other 22 plant-specific AGCVIII kinases in *Arabidopsis* is that they have a stretch of 36 to 90 additional amino acids between subdomain VII and VIII of the catalytic kinase domain, which we named the insertion domain (ID, (Rademacher and Offringa, 2012)). Previously, it was shown for PID that the PM association domain localizes to this ID (Zegzouti et al., 2006b). As our own analysis already showed that TCH3 binds to the catalytic kinase domain of PID (Chapter 2), and this interaction is able to shield off the PM association domain, we focused our search for the TCH3 binding domain to the ID of PID. Through protein modelling and extensive deletion and amino acid substitution mapping we were able to pinpoint both the PM association domain and the TCH3 binding domain to the same amino acid stretch comprising an amphipathic alpha helix/IQ-like domain. Although we were not able to generate the desired untouchable PID version, this research revealed a dual interaction domain that allows an elegant novel mechanism of regulation of the activity of PID kinase activity, through the Ca^{2+}-dependent removal of the kinase from the PM, away from its phosphorylation targets, the PIN proteins.

Results

PID interacts with TCH3 and closely-related CMLs

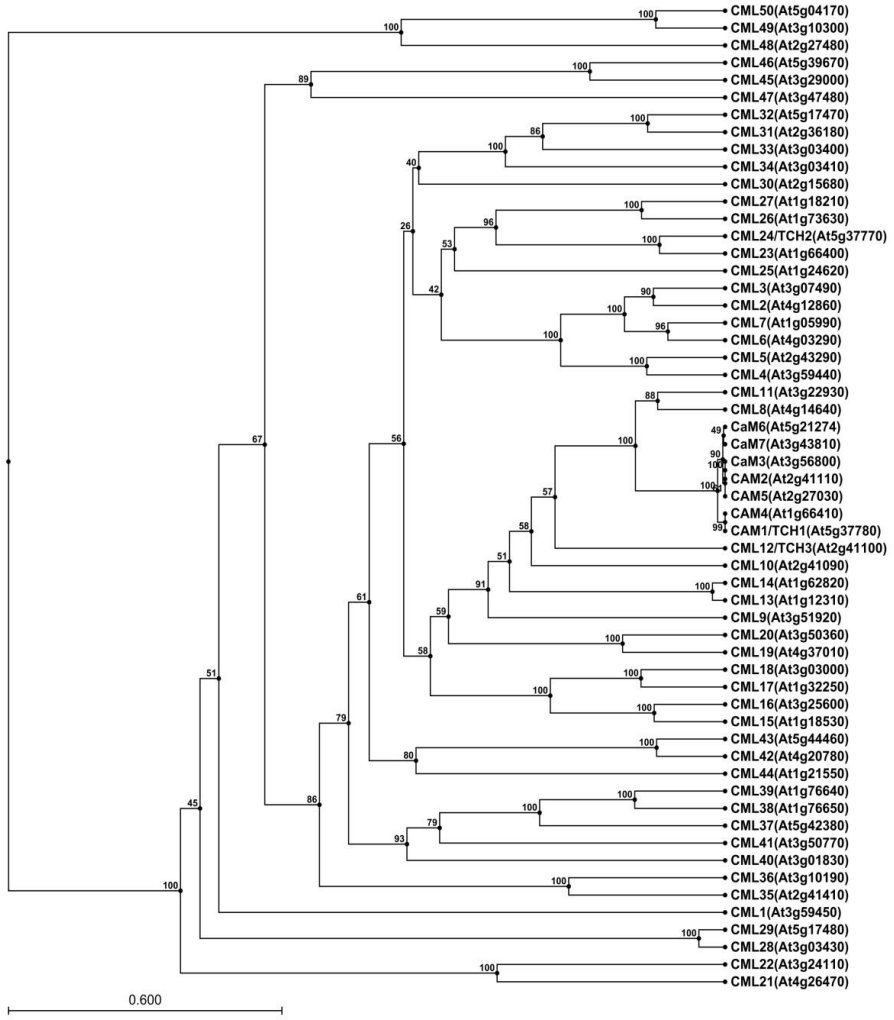

Figure 1. Phylogenetic tree of the *Arabidopsis* calmodulins (CaMs) and calmodulin-like proteins (CMLs).

The phylogenetic tree was constructed by the UPGMA method. CaM and CML amino acid sequences were obtained from the TAIR database (http://www.Arabidopsis.org/). The TCH3 amino acid sequence used for constructing the phylogenetic tree comprises EF hands 3 to 6 (101-255 aa). For all other CAMs and CMLs the full amino acid sequence was used. The bootstrap values are given on the nodes as percentages. The scale depicts 0.6 substitutions per position.

In Chapter 2 we showed that auxin triggers sequestration of the protein kinase PINOID (PID) from the PM to the cytosol through a Ca^{2+}-dependent interaction with the CML TCH3. Internalization of PID-VENUS was significantly reduced in the *tch3-3* mutant a few minutes after auxin treatment, but after 20 minutes full internalization could be observed in this mutant background, suggesting that other CMLs or even the closely related CaMs act redundantly with TCH3 in this process. A recent protein interaction study using seven more divergent *Arabidopsis* CaM/CMLs identified 173 CaM/CMLs interacting proteins, of which 25% interact with all seven CaM/CMLs (Popescu et al., 2007). In view of these data, we tested the interaction of PID with other CaM/CMLs. Based on a phylogenetic tree of the CaMs and CMLs (Figure 1), we selected the most closely related to CML12/TCH3, CML10 (At2g41090) and one more distantly related CML24/TCH2 (At5g37770) and tested these proteins for binding with PID. Interestingly, like *TCH3*, also the *TCH2* gene has been identified in a screen for touch-inducible genes (Braam and Davis, 1990).

Co-transfection of *Arabidopsis* protoplasts with *35S:CFP* and *35S::TCH2-YFP* or *35S::CML10-YFP* showed that, like TCH3-YFP, both TCH2-YFP and CML10-YFP localize to the cytoplasm, and that in contrast to CFP these fusion proteins are excluded from the nucleus (Figures 2A,D). This localization differed significantly from that of PID-CFP, which is predominantly PM-associated both in protoplasts and *in planta* (Chapter 2 and Figure 2B).

When *35S::PID-CFP* and *35S::CML10-YFP* were co-transfected in auxin-starved *Arabidopsis* protoplasts, the subcellular location of PID-CFP did not change (Figure 2B). However, when the cotransfected cells were cultured in normal auxin-containing medium, PID-CFP subcellular localization became cytoplasmic (Figure 2C), suggesting that the auxin-dependent interaction with CML10 sequesters PID from the PM. In contrast, when *35S::PID-CFP* and *35S::TCH2-YFP* were co-transfected, either in auxin-starved or in auxin-cultured *Arabidopsis* protoplasts, PID-CFP remained at the PM (Figure 2E, F). This data suggests that PID interacts with CML10, but not with the more distantly related TCH2.

In order to confirm these results, we analyzed the interaction by cotransfecting protoplasts with *35S::PID-CFP* and *35S::TCH3-YFP*, *35S::CML10-YFP* or *35S::TCH2-YFP* and using the sensitized emission approach to detect Fluorescent Resonance Energy Transfer (FRET) between the two fluorophores. While strong FRET was detected in protoplasts transfected with the positive control construct *35S::CFP-YFP*, a much lower but significant FRET signal was detected in protoplasts

co-expressing PID-CFP and one of the CML-YFP fusion proteins, relative to their corresponding negative control (protoplasts co-expressing CFP and the corresponding CML-YFP (Figure 2G). In protoplasts co-expressing PID-CFP and TCH2-YFP, the FRET index was lower than for the other two combinations, suggesting that PID and TCH2 interact only with low affinity.

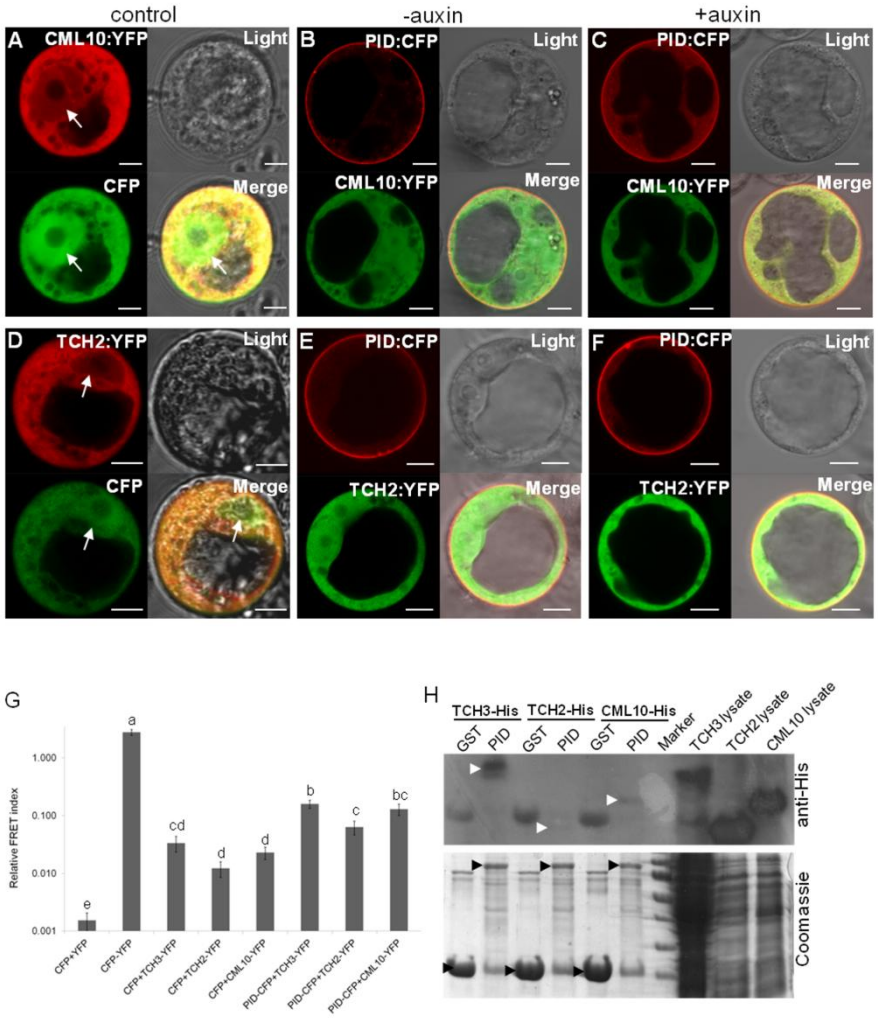

Figure 2. PID is efficiently sequestered from the PM through binding with TCH3 and the closely related calmodulin-like protein CML10, but not with the more distantly related CML24/TCH2.

(A-F) *Arabidopsis* control protoplasts co-transfected with *35S::CML10-YFP* and *35S::CFP* (A) or

35S::TCH2-YFP and *35S::CFP* (D), showing that CML10-YFP and TCH2-YFP are cytoplasmic and excluded from the nucleus (white arrows). Auxin-starved (B,E) or auxin-cultured (C,F) *Arabidopsis* protoplasts co-transfected with *35S::PID-CFP* and *35S::CML10-YFP* (B,C) or with *35S::PID-CFP* and *35S::TCH2-YFP* (E,F). PID sequestration to the cytoplasm can be observed in auxin-cultured protoplasts co-expressing CML10, but not TCH2. For each protoplast in A-F confocal images are shown of the individual CFP-, YFP- and transmitted light channels and of the three channels merged. The scale bar indicates 10 μm. (G) Sensitized emission analysis of Fluorescent Resonance Energy Transfer (FRET) between PID-CFP and TCH3-YFP, TCH2-YFP or CML10-YFP. Protoplasts co-expressing CFP with YFP, TCH3-YFP, TCH2-YFP or CML10-YFP are used a negative control, and protoplasts expressing a CFP-YFP fusion as positive control. The graph shows the relative FRET index on a logarithmic (log^{10}) scale. The values are compared and classified (a to e) using the Student's *t*-test ($P<0.05$). (H) *In vitro* pull down assay using GST or GST-PID bound to glutathione beads as bait. His-tagged fusions of TCH3 and CML10 show a significant interaction, whereas only a very weak interaction is observed for TCH2. Upper panel: Western blot detecting His-tagged CML proteins using anti-His antibodies. White arrowheads indicate the positions of the His-tagged CML proteins. The anti-His antibody shows cross-reaction with the dominant GST band. Lower panel: Coomassie stained gel showing the protein input in the pull-down assay. Black arrowheads indicate the band representing GST (lower) or GST-PID (upper).

In order to further confirm the interaction, GST-tagged isolates of full-length PID were incubated with crude *E.coli* extracts containing Histidine (His)-tagged TCH3, TCH2 or CML10. Protein complexes were pulled down with glutathione beads and separated on gel. Western blot analysis using anti-His antibodies showed that PID interacts most strongly with TCH3, significantly with CML10 and only very weakly with TCH2 (Figure 2H).

These data are in line with our hypothesis that CML10 and other closely related CMLs act redundantly with TCH3 in sequestering PID from the PM through their Ca^{2+}-dependent interaction with this kinase. Based on FRET and *in vitro* pull downs, the more distantly related CML TCH2 does bind to PID, but with insufficient affinity to sequester PID from the PM. This role seems to be reserved for TCH3 and the more closely related CMLs. The results explain why NAA-induced PID internalization is still observed in the *tch3-3* mutant background, and also why the *tch3-3* loss-of-function mutant does not show a strong phenotype.

CaM/CML binding and PM-association are mediated by the PID insertion domain

In Chapter 2 we demonstrated a function for the PID-TCH3 interaction during gravitropic root growth, however, the effect of the *tch3* loss-of-function on root gravitropism was mild, probably because other redundantly interacting CML proteins are also expressed in the root tip. One way to obtain a clearer view on the function of the PID-CML signaling complex in plant development would be to complement the *pid* loss-of-function mutant with a PID mutant version that is fully functional except for its interaction with the CMLs (untouchable PID). We therefore set out to map the CML-binding domain in PID.

A typical characteristic of the plant-specific AGCVIII kinases is that they have an insertion of about 36-90 amino acids in their catalytic domain (Galván-Ampudia and Offringa, 2007; Rademacher and Offringa, 2012) For PID this ID was reported to be involved in its association with the PM (Zegzouti et al., 2006b; Galván-Ampudia and Offringa, 2007; Rademacher and Offringa, 2012). In order to confirm these initial localization studies in yeast, we constructed an ID-YFP fusion and transfected this to *Arabidopsis* protoplasts. Like PID-YFP, also ID-YFP showed predominant PM localisation (Figure 3C, D), confirming that PID associates with the PM through its ID.

Previous analysis showed that TCH3 interacts with the catalytic domain of PID (Chapter 2). As TCH3 binding interfered with the association of PID to the PM, we tested the hypothesis that TCH3 binds to the PID ID. Indeed, TCH3 could be pulled down *in vitro* by GST-PID or even stronger with the GST-ID alone, but not by a GST-PID versions whose ID had been removed (PID minus ID, Figure 3A, B). Placing back the ID in PID minus ID (PID-ID+ID) restored its capacity to pull down TCH3 (Figure 3A, B). Taken together, our results strongly indicated that both the PM association domain and the CaM/CML binding domain are located inside the ID of PID.

To further map the CaM/CML binding domain, we replaced the ID with three smaller segments, being 227-253, 240-266, 254-280 (PID-ID+$ID_{227-253}$ etc., Figure 3A). The *in vitro* pull down experiments showed that the $ID_{240-266}$ segment strongly bound to TCH3, whereas the other segments did not (Figure 3G), suggesting that the calmodulin binding domain is located in the middle part of the ID.

When expressed in *Arabidopsis* protoplasts, PID-YFP, PID-ID+ID:YFP and PID-ID+$ID_{240-266}$:YFP localized to the PM (Figure 3H, I, L), whereas the PID-ID:YFP, PID-ID+$ID_{227-253}$:YFP and PID-ID+$ID_{254-280}$:YFP fusions localized to the cytosol (Figure 3E, F, J, K, M). This result suggests that the PM binding domain and the CaM/CML binding domain overlap in the middle segment of the ID. In some protoplasts PID versions with ID deletions localized to cytoskeleton-like stuctures

(Figures 3E and J), suggesting that in the absence of PM association or TCH3 binding PID can be recruited to the cytoskeleton.

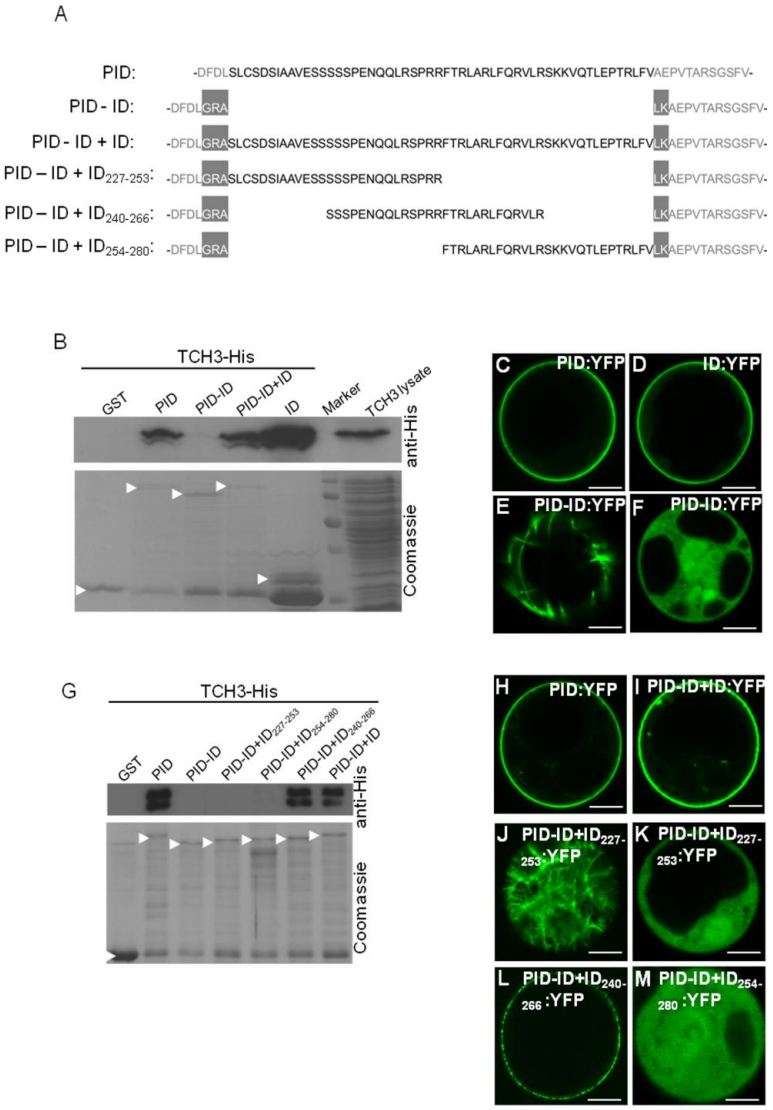

Figure 3 CaM/CML binding and PM association are mediated by the middle part of the PID ID

(A) An overview of the PID ID (black letters) with different PID mutant versions used in the *in vitro* pull down and protoplast expression experiments. The mutant PID versions were generated by creating restriction

enzyme sites, which introduced a few additional amino acids at the borders of the ID (boxed in gray).
(B) *In vitro* pull down of His-TCH3 with GST, GST-PID (PID), GST-PID without ID (PID-ID), GST-PID minus ID with the ID placed back (PID-ID+ID) or with GST-ID (ID). Upper panel: Western blot analysis using anti-His antibodies to detect His-tagged TCH3. Lower panel: Coomassie stained gel showing sample loading. The size marker and TCH3 lysate are loaded as reference. White arrowheads indicate the positions of the respective GST-tagged proteins.
(C-F) *Arabidopsis* protoplasts expressing PID-YFP (C), ID-YFP (D) or PID minus ID-YFP (E, F)
(G) *In vitro* pull down of His-TCH3 with GST, GST-PID (PID), GST-PID minus ID (PID-ID), GST-PID minus ID with the ID segments 227-253, 254-280, 240-266 or the complete ID re-inserted (PID-ID+$ID_{227-253,}$ PID-ID+$ID_{254-280,}$ PID-ID+$ID_{240-266,}$ or PID-ID+ID). Upper panel: Western blot analysis using anti-His antibodies to detect His-tagged TCH3. Lower panel: Coomassie stained gel showing sample loading. White arrowheads indicate the positions of the respective GST-tagged proteins.
(H-M) *Arabidopsis* protoplasts expressing a PID-YFP fusion (H), or a PID minus ID-YFP fusion with the ID segments 227-253 (J, K), 240-266 (L), 254-280 (M), or the complete ID (I) re-inserted.
C-F and H-M show confocal YFP channel images. The scale bar indicates 10 μm.

To fine map the PM and TCH3 binding domains, we used alanine scanning to replace stretches of 7 amino acids in the middle part of the ID, being Ala1 (QLRSPRR), Ala2 (FTRLARL), Ala3 (FQRVLRS) (Figure 4A). In general, CaM/CML binding domains are enriched in hydrophobic and positively charged amino acids (Poovaiah et al., 2013), and we therefore ignored the first part of this fragment (SSSPENQ), as it contains no positively charged amino acids and only one hydrophobic residue. Surprisingly, none of the three Ala mutants showed PM localization (Figure 4B-F), nor did they show *in vitro* binding to TCH3 (Figure 4G). This data confirms that the middle part of the ID is both important for CaM/CML binding and for association of the kinase to the PM. Interestingly, besides showing cytoplasmic localization, the PID Ala2-CFP mutant localized to endosomal compartments (Figure 4D), and the PID Ala3-CFP mutant to cytoskeleton-like structures (Figure 4E). These results corroborate our previous findings that PID subcellular localization is dynamically regulated (Chapter 2), and that PID can be recruited to other subcellular compartments, such as endosomes or the cytoskeleton, when PM association or TCH3 binding is disrupted.

An amphipathic alpha helix in the PID insertion domain mediates both CaM/CML binding and PM association

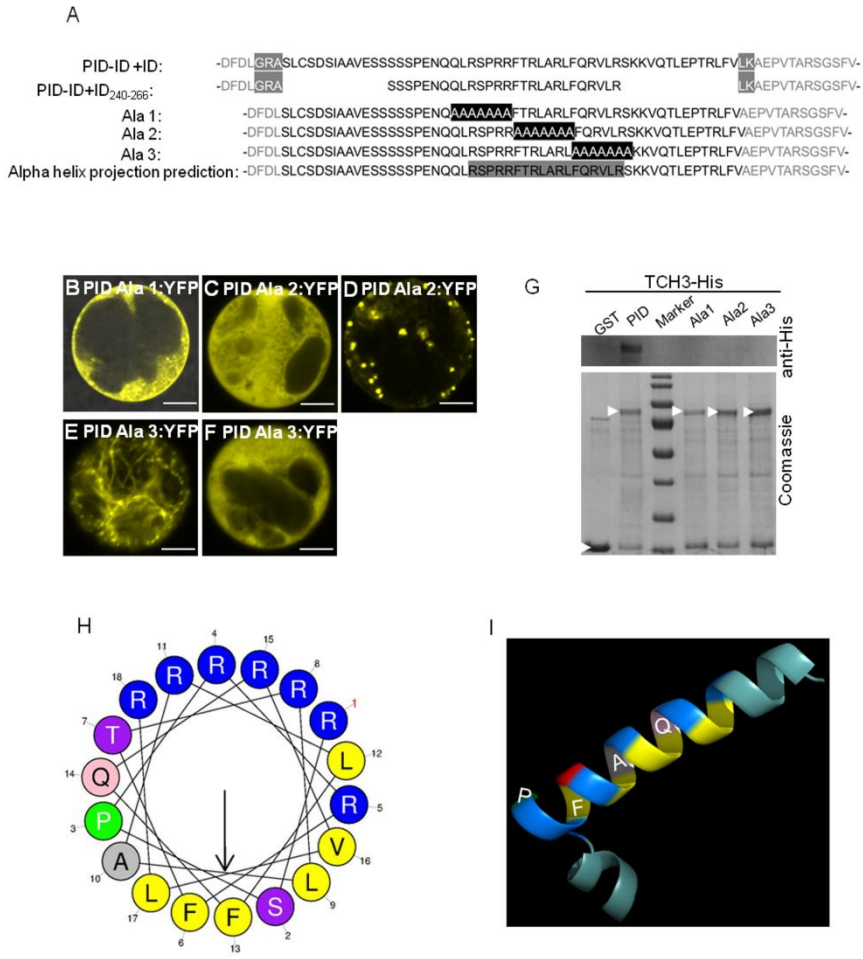

Figure 4 Alanine scanning and protein structure prediction suggest that PM association and CaM/CML binding are mediated by an amphipathic alpha helix in the PID ID.

(A) An overview of the amino acid changes in the ID of different PID mutant proteins. The ID is represented by black letters. The white letters in gray background indicate the additional amino acids introduced by the addition of restriction enzyme sites in the construct. The white letters in black background indicate the amino acid stretches substituted by alanines. The black letters in grey background indicate the position of the predicted amphipathic alpha helix. (B-F) *Arabidopsis* protoplasts expressing alanine substitution versions PID Ala1-YFP (B), PID Ala2-YFP (C, D), PID Ala3-YFP (E, F). Scale bars indicate 10 μm.

(G) *In vitro* pull down of His-tagged TCH3 with GST, GST-tagged PID (PID), GST-tagged PID Ala1 (Ala1), GST-tagged PID Ala2 (Ala2) or GST-tagged PID Ala3 (Ala3). Upper panel: Western blot analysis using

anti-His antibodies to detect His-tagged TCH3. Lower panel: Coomassie stained gel showing sample loading. White arrowheads indicate the positions of the respective GST-tagged proteins.

(H, I) Alpha helix projection (H) and protein structure prediction indicate that amino acid residues 249 to 266 in PID form a strong amphipathic alpha helix. Positively charged residues are in blue, whereas the hydrophobic residues are in yellow or grey. The numbers 1 to 18 in (H) indicate the order of the amino acids in the sequence. (I) 3D protein structure prediction of the amphipathic alpha helix (residues 249 to 266) with a positively charged face (blue) on one side and a predominantly hydrophobic face (yellow/grey) on the other side. The same color code for the amino acid residues is used in (H) and (I), except that the threonine residue (purple in H) is now red.

Ca^{2+}-dependent CaM binding is generally mediated by a non-conserved domain of around 20 amino acids with multiple basic residues flanking critical hydrophobic residues, and often a propensity to form an amphipathic alpha helix (Poovaiah et al., 2013). Ca^{2+} binding by a CaM results in conformational changes that exposes hydrophobic residues that wrap around the hydrophobic residues in this amphipathic helix, while acidic residues interact with the basic residues in the amphipatic helix (Snedden and Fromm, 2001; Bahler and Rhoads, 2002; Du and Poovaiah, 2005; Poovaiah et al., 2013). Moreover, amphipathic helices have also been reported to mediate interaction of peripheral membrane proteins with phospholipids in the PM (Heximer et al., 2001; Bhardwaj et al., 2013; Lu and Taghbalout, 2013).

In view of the overlapping CaM/CML binding and PM association functionalities in the PID ID, we looked more closely to its 3 dimensional structure. Several protein structure tools predicted the presence of an alpha helix inside of the ID (Figure 4A). Visualization of this alpha helix using helical wheel projection software (http://heliquest.ipmc.cnrs.fr/) indicated that the ID segment comprising amino acid residues 249 to 266 (RSPRRFTRLARLFQRVLR) forms a perfect amphipathic alpha helix with seven positively charged amino acids on one side, and six hydrophobic amino acids on the other side (Figure 4A, H, I).

To confirm that the predicted amphipathic alpha helix is important for CaM/CML binding and PM localization, we generated the PID mutants R249,252,253A,R263,266A, R249,252,253,263,266A in which the amphipathic properties of the helix were disrupted, and used PID mutant S/T250, 255A, which is not changed in the amphipathic properties but has potential phosphorylation sites removed, as a negative control. Transfection of the constructs *35S::PID*$_{R249,252,253A}$*-YFP*, *35S::PID*$_{R263,266A}$*-YFP*, *35S::PID*$_{R249,252,253,263,266A}$*-YFP* and *35S::PID*$_{S/T250,\ 255A}$*-YFP* to

Arabidopsis protoplasts, showed that all arginine to alanine substitutions disrupted PM localization, whereas the serine/threonine to alanine substitutions did not affect PM localization of PID (Figure 5A-E). The *in vitro* pull-down experiments showed that all R to A substitutions also disrupted the interaction with TCH3, whereas the S/T250, 255A substitutions did not. Our results indicate that the amino acid residues 249 to 266 in the ID of PID form an amphipathic alpha helix that mediates both CaM/CML binding and PM association.

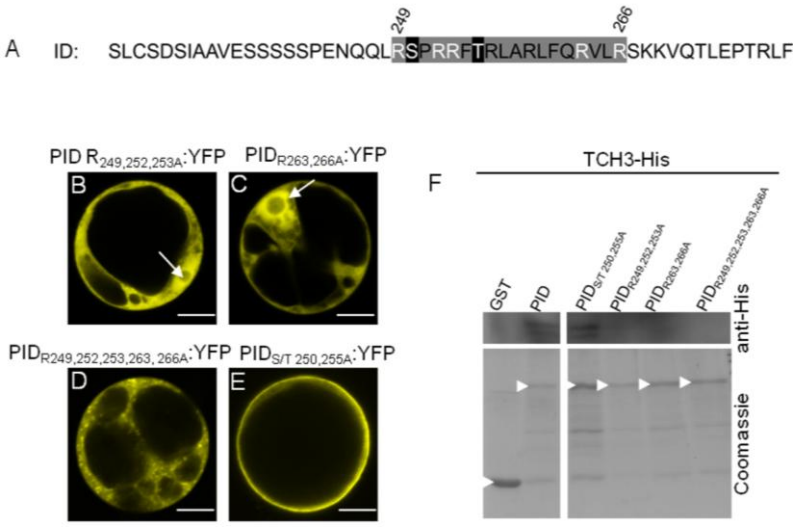

Figure 5 Amphipathic properties of the alpha helix in the PID ID are important for both PID PM localization and CaM/CML binding.

(A) An overview of the PID ID, with the amino acid residues comprising the predicted amphipathic alpha helix highlighted by a grey box, and the arginines (R) or the serine or threonine (S/T) that were substituted by alanines indicated by white letters. (B-E) *Arabidopsis* cell suspension protoplasts expressing $PID_{R249,252,253A}$-YFP (B), $PID_{R263,266A}$-YFP (C), $PID_{R249,252,253,263,266A}$-YFP (D) or $PID_{S/T\ 250,255A}$-YFP (E). Size bars indicate 10 µm. (F) *In vitro* pull down of His-tagged TCH3 with GST, or GST-tagged PID (PID), -$PID_{R249,252,253A}$, -$PID_{R263,266A}$, -PID $_{R249,252,253,263,266A}$ or -$PID_{S/T\ 250,255A}$. Upper panel: Western blot analysis using anti-His antibodies to detect His-tagged TCH3. Lower panel: Coomassie stained gel showing sample loading. White arrowheads indicate the positions of the respective GST-tagged proteins.

An IQ-like motif overlapping with the amphipathic alpha helix is required for CaM/CML binding *in vivo*

Our previous data showed that the $ID_{240\text{-}266}$ fragment containing the amphipathic alpha

helix was sufficient to confer PM localization to the PID-ID+$ID_{240-266}$ fusion protein (Figure 3L), and also to efficiently pull down TCH3 *in vitro* (Figure 3G). However, co-transfection of *Arabidopsis* protoplasts with *35S::PID-ID+$ID_{240-266}$-CFP* and *35S::TCH3-YFP* showed that this part of the ID cannot be sequestered by TCH3, even in auxin-treated *Arabidopsis* protoplasts (Figure 6A, D, E), whereas the PID-CFP control showed clear auxin-dependent sequestration (Figure 6B, C). These data corroborate that the PM association domain maps to this middle segment of the ID, but also indicate that this segment is not sufficient for efficient binding of TCH3 or related proteins *in vivo*.

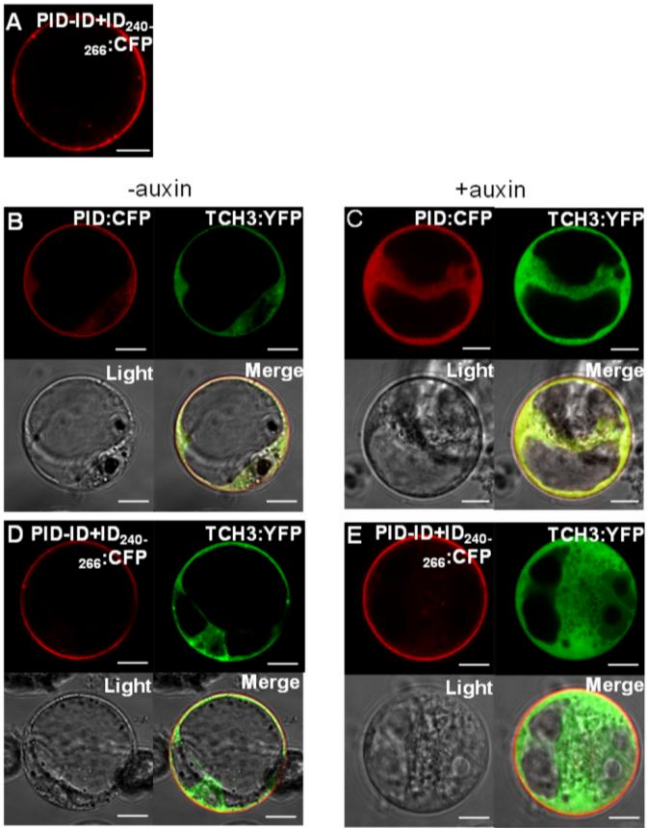

Figure 6 The amphipathic alpha helix in the PID ID is not sufficient for TCH3-mediated sequestration of PID from the PM in *Arabidopsis* protoplasts.

(A) Confocal images (CFP channel) of *Arabidopsis* protoplasts expressing PID-ID+$ID_{240-266}$-CFP. (B-E) Auxin-starved (B, D) or auxin-cultured (C, E) *Arabidopsis* protoplasts co-expressing TCH3-YFP and

PID-CFP (B,C) or TCH3-YFP and PID-ID+$ID_{240-266}$-CFP (D,E). For each protoplast in B-E the confocal images of the individual CFP-, YFP- and transmitted light channels and of the three channels merged are shown. Scale bar indicates 10 µm.

Further analysis of the PID ID for putative CaM/CML binding domains identified an IQ-like motif that partially overlaps with the amphipathic alpha helix (Figure 7A). IQ motifs can be found in a wide range of CaM target proteins, where they can mediate either Ca^{2+}-dependent or Ca^{2+}-independent interactions with the CaM (Rhoads and Friedberg, 1997; Bahler and Rhoads, 2002). The IQ-like motif identified in PID lacks the central G residue and also the second basic residue that is normally found in Ca^{2+}-independent IQ-motifs, which fits with its Ca^{2+}-dependent action (http://calcium.uhnres.utoronto.ca/ctdb/ctdb/motifs/iq_motif.html; (Houdusse and Cohen, 1995; Munshi et al., 1996)).

To test whether the predicted overlapping amphipathic alpha helix and IQ-like motif together were required for the interaction with TCH3 *in vivo*, a fragment encoding amino acid residues 244 to 275 (ENQQLRSPRRFTRLARLFQRVLRSKKVQTLEP) was translationally fused to YFP. The $ID_{244-275}$-YFP fusion showed PM localization (Figure 7A, B), like PID-YFP and ID-YFP, and the $ID_{244-275}$-YFP fusion protein was sequestered to the cytosol in an auxin-dependent manner when co-expressed with TCH3-CFP (Figure 7C-H). This data suggests that the fragment contains a functional CaM/CML binding and PM association domain, and that the additional amino acids belonging to the predicted IQ-like motif are essential for CaM/CML binding *in vivo* .

Interestingly, we noted that when the ID-YFP and the $ID_{244-275}$-YFP fusion proteins were co-expressed together with TCH3-CFP, they showed significantly more cytoplasmic signal in the auxin-starved protoplasts compared to full length PID-YFP (Figure 7C-H), and also compared to when the fusion proteins were expressed alone (Figure 7A). This suggests that TCH3 has higher affinity for the ID fragments compared to the full length PID protein, which possibly causes TCH3 to interact with these fusion proteins even in the absence of the auxin-induced Ca^{2+} signal. Indeed, the *in vitro* pull down experiments confirmed that the affinity of TCH3 for the $ID_{244-275}$-GST fusion is significantly higher than for the PID-GST fusion (Figure 7I). This result implies that access of TCH3 to the ID is somehow inhibited by the rest of the PID protein, and that an auxin-triggered Ca^{2+} response is required for efficient recruitment of PID by TCH3. Interestingly, in an *in vitro* pull down assay the GST-tagged $ID_{244-275}$ showed interaction with TCH3 and the closely-related CAM2, but not with CML9, and only weakly with the even less-related

calmodulin-like protein TCH2 (Figure 7J). In view of the strong amino acid conservation among the seven CAMs in *Arabidopsis* (Figure 9), it is likely that they all interact with PID. Our results suggest that the CAMs and the closely related CMLs TCH3 and CML10 act redundantly in regulating the activity of PID and WAG2, by sequestering these kinases from the PM in response to elevated cytosolic calcium levels ($[Ca^{2+}]_{cyt}$).

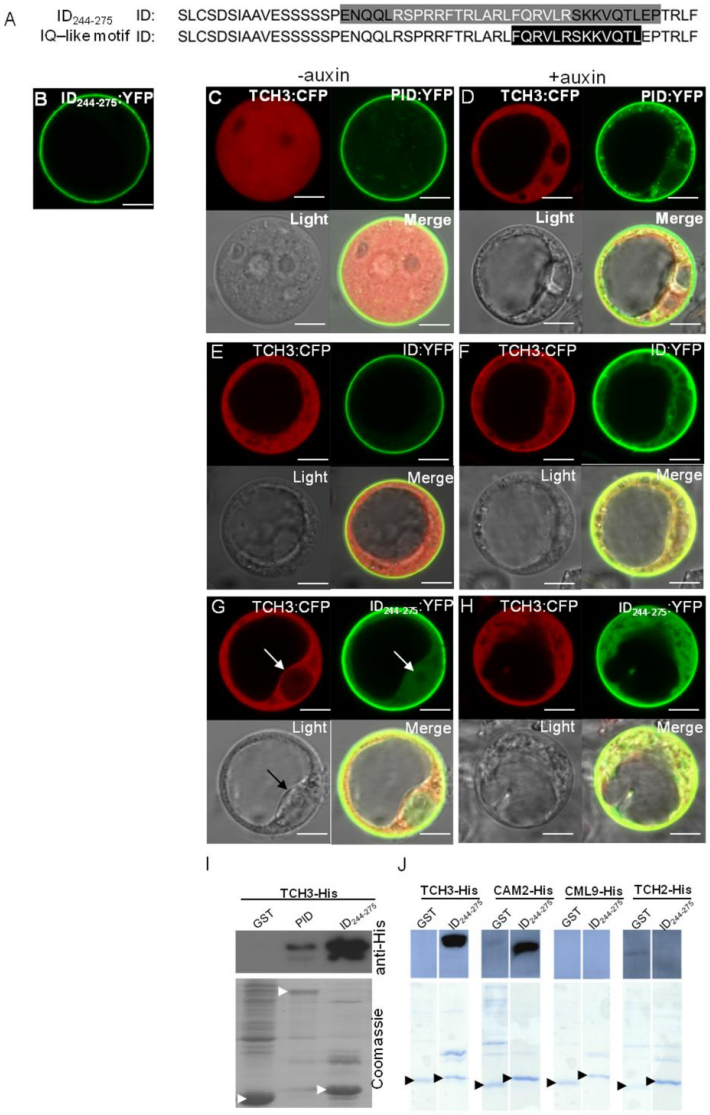

Figure 7 A segment of the PID ID comprising the amphipathic alpha helix and the overlapping IQ-like Motif is sufficient for PM association and auxin-triggered CaM/CML-mediated sequestration.

(A) An overview of the PID ID with the amino acid residues of the $ID_{244-275}$ segment highlighted by a grey box, and the IQ-like motif indicated by white letters in a black box. The white letters in the grey box indicate the predicted alpha helix.

(B) Confocal image (YFP channel) of *Arabidopsis* protoplast expressing $ID_{244-275}$-YFP. (C-H) Auxin-starved (C, E, G) or auxin-cultured (D, F, H) *Arabidopsis* protoplasts co-expressing TCH3-CFP and PID-YFP (C,D), TCH3-CFP and ID-YFP (E,F), or TCH3-YFP and $ID_{244-275}$-YFP (G,H). For each protoplast in C-H confocal images are shown of the individual CFP-, YFP- and transmitted light channels and of the three channels merged. Scale bar indicates 10 µm. White arrow in G indicates the nucleus.

(I, J) *In vitro* pull down of His-tagged TCH3 with GST, or GST-tagged PID or -$ID_{244-275}$ (I) or of His-tagged TCH3 , -CAM2, -CML9 or -TCH2 with GST, or GST-tagged $ID_{244-275}$ (J). Upper panel: Western blot analysis using anti-His antibodies to detect His-tagged TCH3. Lower panel: Coomassie stained gel showing sample loading. White (I) or black (J) arrowheads indicate the positions of the respective GST-tagged proteins.

PM association and CaM binding are tightly coupled functionalities in the PID ID

The $ID_{240-266}$ fragment was sufficient for PM association, but sequestration by TCH3 in protoplasts required the $ID_{244-275}$ segment, which included the IQ-like motif. As expected, deletion of the complete IQ-like motif or substitution of the motif for alanines disrupted both PID PM association and its interaction with TCH3 (M3 and M4, Figure 8A,E,F,J). We hypothesized, however, that it should be possible to disrupt the interaction between PID and TCH3 without interfering with PID PM-association by substituting residues in the IQ-like motif that are not part of the predicted amphipathic alpha helix. We focused on positively charged and hydrophobic amino acids, as these are known to be important for the interaction with the CaMs and CMLs (Snedden and Fromm, 2001; Du and Poovaiah, 2005; Du et al., 2009). Unexpectedly, all mutant PID versions (M1, M2, M5, M6 and M7) had lost their capacity to associate to the PM (Figure 8A-I), whereas two IQ-like motif-specific substitutions (M6 and M7) were still able to interact with TCH3 in *in vitro* pull downs (Figure 8A, J). Since the *in vivo* assay for CaM/CML-mediated sequestration requires PID to be at the PM, we cannot exclude that efficient *in vivo* CaM/CML binding does require the complete IQ-like motif (including the VQTL residues).

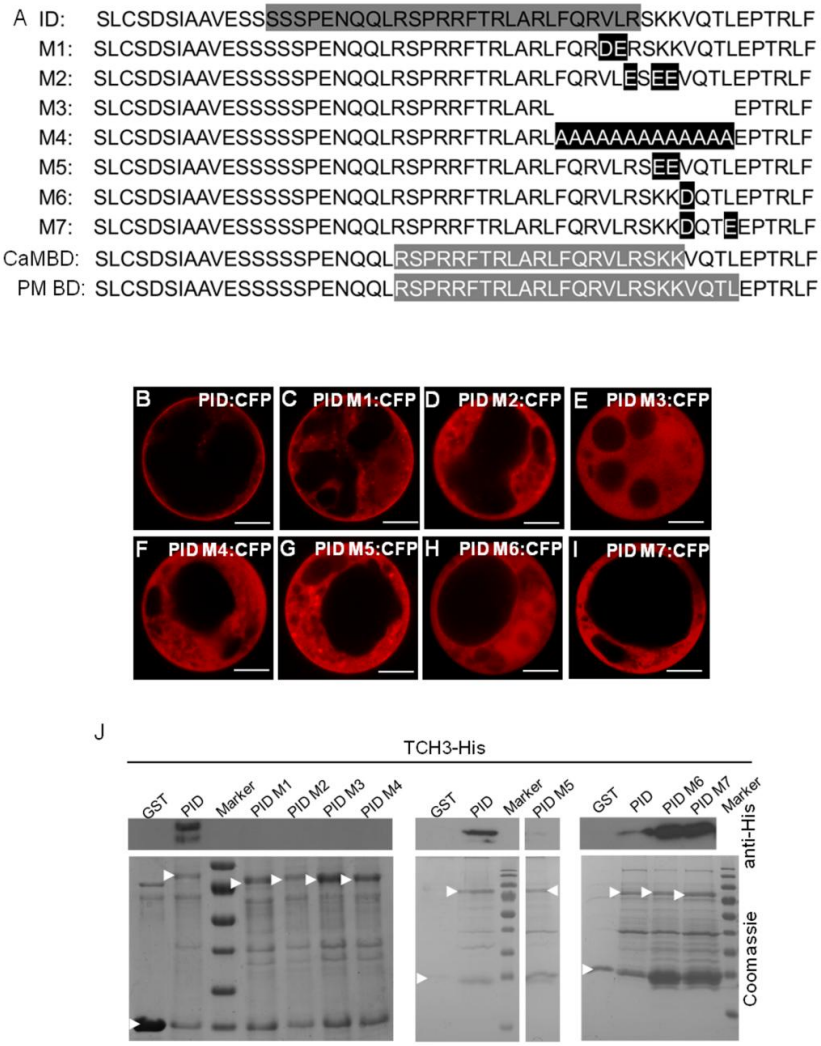

Figure 8 CaM/CML binding and PM association converge at an overlapping amphipathic alpha helix and IQ-like motif in the PID ID.

(A) An overview of the PID ID and the amino acid deletions or substitutions introduced in the mutant versions M1 to M7. The black letters with a grey background indicate amino acids that are the part of the $ID_{240-266}$ segment that seems sufficient for PM localization but not for sequestration by TCH3 binding *in vivo*. The white letters in black background indicate the amino acid substitutions in the PID mutant versions. The white letters with grey background indicate the amino acid region needed for CaM/CML binding (CaM BD) or PM association (PM BD).

(B-I) *Arabidopsis* protoplasts expressing PID-CFP or the mutant versions M1 to M7. The scale bars indicate 10 µm.

(J) *In vitro* pull down of His-tagged TCH3 with GST, or GST-tagged PID or its mutant versions M1 to M7. Upper panel: Western blot analysis using anti-His antibodies to detect His-tagged TCH3. Lower panel: Coomassie stained gel showing sample loading. White arrowheads indicate the positions of the respective GST-tagged proteins.

Based on these data, we concluded that PM association and CaM/CML binding are two tightly associated functionalities present in the ID of PID (PM BD and CaM BD, Figure 8A). Unfortunately, this strong overlap prevents the generation of an untouchable PID, a kinase version that still associates with the PM but cannot be sequestered to the cytosol through the Ca^{2+}-dependent interaction with a CaM or CML. However, our research has identified a novel domain that confers Ca^{2+} responsiveness to the PID kinase by combining the CaM/CML binding and PM association characteristics.

Discussion

The second messenger Ca^{2+} is one of the most elementary signaling molecules in all organisms, that acts through rapid trigger-induced elevation of its cytosolic concentration (Roberts and Harmon, 1992; Trewavas and Malho, 1998; Chin and Means, 2000). In plants, the $[Ca^{2+}]_{cyt}$ is increased in response to diverse stimuli, including the plant hormone auxin (Knight et al., 1991; Polisensky and Braam, 1996; Knight, 2000),. Auxin increases $[Ca^{2+}]_{cyt}$ in root epidermis cells within seconds after application (Monshausen et al., 2011). Ca^{2+} signals are perceived through proteins that recruit Ca^{2+} through specific binding pockets (EF-hands), and subsequently undergo conformational changes that alter their activity (e.g. Ca^{2+}-dependent protein kinases), or allow them to interact with and to (in)activate their target proteins. CaMs are ubiquitous Ca^{2+}-binding proteins that have a double set of two EF hands, and share almost 90% sequence identity across plant, fungal, and vertebrate species (Zielinski, 1998). Based on this high level of sequence conservation, CaMs probably function in a similar way throughout diverse organisms. Next to the seven CAMs, the *Arabidopsis* genome encodes a large family of 50 CMLs that are predicted to act in a similar manner as the CaMs (McCormack and Braam, 2003). After Ca^{2+} binding to the EF-hands, two hydrophobic surfaces in CaM/CMLs surrounded by negative charges will be exposed, and these are able to efficiently interact with a stretch of hydrophobic amino acid residues in the target protein (Snedden and Fromm, 2001). In general, target proteins share very little

amino acid sequence similarity in their CaM/CML binding sites (Snedden and Fromm, 2001).

Closely related CaMs and CMLs act redundantly in Ca^{2+}-dependent sequestration of PID from the PM

In Chapter 2 we showed that Ca^{2+} acts downstream of asymmetric distribution of auxin during root gravitropism. Auxin induced elevation of $[Ca^{2+}]_{cyt}$ led to binding of the CML TCH3 to PID, which recruited this kinase to the cytosol, and led to apolar PIN2 distribution in the root epidermis, needed to maximize the root gravitropic response. Based on these initial findings we investigated whether PID interacts with other CMLs or CaMs. Our data indicates that PID interacts with CML10 and CAM2, both closely related to TCH3. In view of the high amino acid identity it is likely that the other 6 *Arabidopsis* CaMs do also interact with PID. Surprisingly, no interaction was observed with CML9, which is closely related to TCH3 and CML10, and we found only a very weak interaction with the more distantly related CML24/TCH2. These results indicate that the Ca^{2+}-dependent sequestration of PID is an activity that is shared by only a few CaMs/CMLs. Moreover, the fact that TCH3 is able to sequester only two of the four AGC3 kinases corroborates the specificity of this interaction, and suggests some structural conservation between PID and WAG2, which is not apparent based on the primary amino acid sequence.

An alignment of the four CML proteins TCH3, CML10, CML9 and CML24/TCH2 tested here, together with the seven CaMs (Figure 9) confirmed the high level of identity among the CaMs, but also showed the increased amino acid sequence variation in the EF hands of the CMLs. The EF hands are enriched in negatively charged amino acids aspartic acid (D) and glutamic acid (E), which provide the electronegative environment for Ca^{2+} binding (Figure 9). Each EF hand also has 1-3 hydrophobic methionines (M) (Figure 9). Ca^{2+} binding induces a conformational change in the EF hands, that exposes the hydrophobic methyl groups from the methionines, which promotes binding to the hydrophobic regions of the amphiphilic helix/IQ motif in the target protein. From the alignment in Figure 9, it is difficult to predict which amino acid residues in the CaMs and CMLs are crucial for the specific interaction with the PID and WAG2 kinases.

Regulation of peripheral kinase localization through a single domain: a novel concept?

To overcome the redundant interaction between CaMs and PID, we tried to generate a PID mutant protein in which CaM binding, but not the PM-association was disrupted (untouchable PID). In order to do this we mapped the PID CaM binding- and PM association domains in PID. Our analysis showed that both functionalities converge to an overlapping amphipathic alpha helix and IQ-like motif in the PID insertion domain. The amphipatic properties of the alpha helix as well as the hydrophopic residues in the IQ motif appeared to be important for both functionalities, and the fact that even single amino acid changes in the C-terminal part of the IQ-like motif did not result in an untouchable PID version, indicates that it will be difficult to separate the two functionalities. The best candidate for an untouchable PID is the version where the middle part of the PID ID was placed back (PID-ID+$ID_{240-266}$), as it cannot be sequestered by TCH3, but still associates to the PM. This is surprising, since this version lacks the C-terminal part of the IQ motif, which was shown to be required for PM association. Possibly, the amino acid residues downstream of the amphipathic helix in this mutant version (L**K**AEPVT, see Figure 3A) are able to restore PM association but not the function of the IQ motif (S**K**KVQTL in wild-type PID, Figure 3A). Unfortunately, a preliminary test of this mutant version in an *in vitro* phosphorylation assay suggests that it has lost its kinase activity (data not shown).

CaMs/CMLs have numerous target proteins (Yap et al., 2000; Popescu et al., 2007). Among them, CaM-regulated serine/threonine kinases have been best characterized for their mechanism of interaction with CaM (Hoeflich and Ikura, 2002). Either amphipathic alpha helixes or IQ/IQ-like motifs have been identified before as CaM binding sites. In some cases, the IQ motif can form an amphipathic alpha helix, like in scallop myosin (Xie et al., 1994; Houdusse et al., 2006). However, in our case, the IQ-like motif is only half overlapping the clear amphipathic alpha helix that is predicted by our structural analysis. In PID, this amphipathic helix also acts as a membrane binding site, using the hydrophobic face to insert into the lipid acryl chains and the polar face to interact with the polar heads of the lipids and with the solvent (Cornell and Taneva, 2006).

Both protein-PM association and protein-CaMs/CMLs binding are biochemical processes and dependent on the physicochemical properties of protein, PM and CaMs/CMLs. Preliminary data suggest that PID can interact with the negatively charged phosphoinositides PI(3)P, PI(4)P, PI(5)P, PI(3,5)P2 and PI(4,5)P2 ((Zegzouti et al., 2006a);data not shown) that are found in plant cell membranes (Munnik and Nielssen, 2011). Phosphoinositides could produce the negative field needed to attract proteins

with a positive patch, which could thus mediate PID localization to the PM (Olivotto et al., 1996). The CaMs/CMLs are also enriched in negative charges especially in EF hands (Figure 9). So both the negatively charged CaMs/CMLs and phosphoinositides may competitively interact with the positive charges on the amphiphitic alpha helix/IQ-like motif, which may be the reason CaMs/CMLs can pull the positive charged amphiphitic alpha helix/IQ-like motif off the PM (McLaughlin and Murray, 2005; Clapham, 2007).

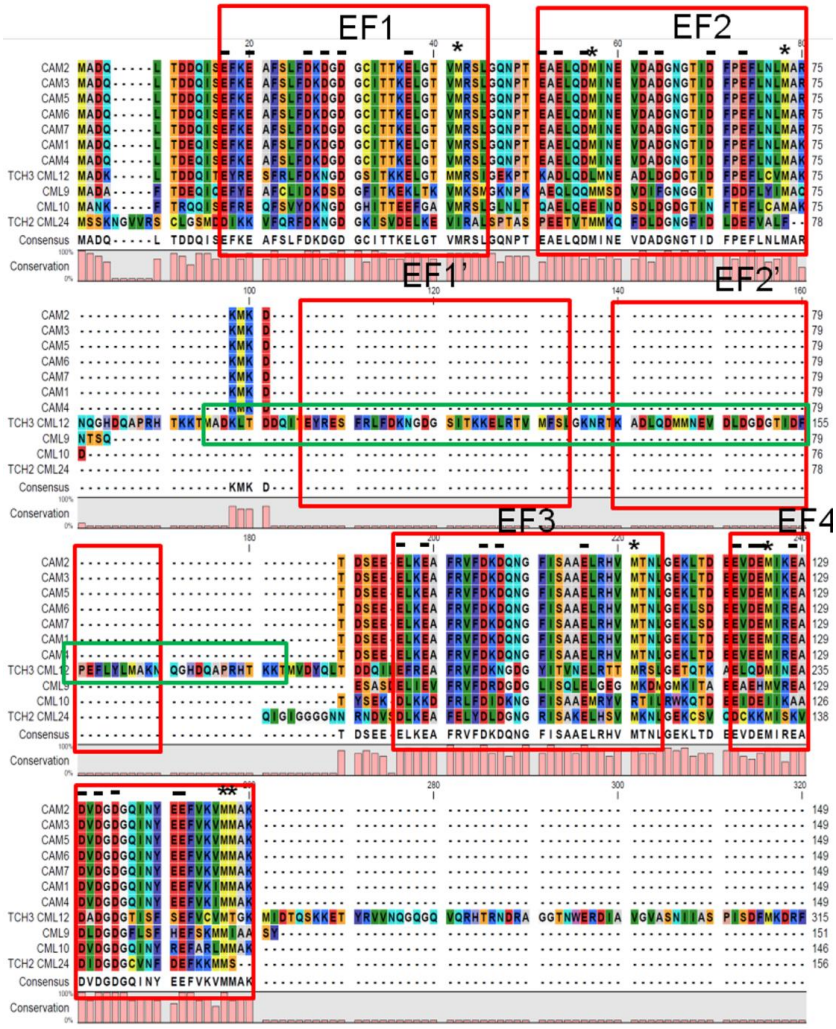

Figure 9 Alignment of TCH3 with CML9, CML10,TCH2 and CAM1 to CAM7.

The red boxes indicate the positions of the EF-hands. The '-' above the alignment indicates negatively charged amino acids in the EF-hands which may be involved for the ion coordination. The methionine residues are marked with '*'.

The dual function of a protein domain in PM association and CaM binding is not a novel concept, as it has been reported for some animal PM associated or transmembrane proteins, but in those cases it just consisted of a cluster of positively charged residues (McLaughlin and Murray, 2005). One example is myristoylated alanine-rich C-kinase substrate (MARCKS), an amorphous protein that besides the basic cluster binds to the PM through a myristylated PM anchor. MARCKS has been shown to specifically associate with PIP2, and its proposed function is to control the level of free PIP2 in the PM dependent on the $[Ca^{2+}]_{cyt}$ through its interaction with CaMs (McLaughlin and Murray, 2005). Other examples are the NMDA and EGF receptors, for which recruitment of the basic cluster by a CaM is used to regulate their activity in a Ca^{2+}-dependent manner (McLaughlin and Murray, 2005).

For PID, the combination of positively charge and the amphipathic helix might be required to guarantee tight binding to the PM, most likely through phosphoinositides, as in contrast to the animal proteins presented above this is the only domain that holds the protein at the PM. Around 14 phosphoinositide binding modules have been identified, most in animal systems (Stahelin et al., 2014), and the combined phosphoinositide binding and CaM/CML binding motif present in PID is certainly a new one. To be able to compete for the tight association of PID with the PM, the CaM/CML requires a high affinity binding site, and this is probably why the combined amphipathic helix /IQ motif in PID has evolved. When expressed in protoplasts, PID is mostly PM associated, whereas the WAG kinases and especially AGC3-4 also show nuclear localization. Further analysis of these kinases should reveal the relevance of this differential localization. At least for PID, and also for WAG2, in view of the redundancy between the CaMs/CMLs and their likely pleitropic function in different signaling pathways, constructing an untouchable version will still be crucial in unraveling the role of the Ca^{2+}-dependent sequestration to the cytosol during plant development.

Experimental procedures

Molecular cloning and constructs

Molecular cloning was performed following standard procedures (Sambrook, 1989).

Bacteria were grown on LC medium containing corresponding antibiotics for *E.coli* strains DH5α, DH10B. Design of molecular cloning, DNA sequence analysis and DNA alignments were performed using the Vector NTI 10 software (Invitrogen).

The constructs *pET16H-TCH3*, *pGEX-PID*, *pART7-TCH3-YFP*, *pART7-PID-CFP*, *pDONR-PID*, *35S::CFP* were described in Chapter 2. The *pART7-PID-YFP* was constructed by LR reaction from *pDONR-PID* to *pART7-Gateway-YFP*. The *pART7-TCH3-CFP* was constructed by LR reaction from *pDONR-TCH3* to *pART7-Gateway-CFP*.

The cDNAs of *TCH2*, *CML10*, *CAM2* and *CML9* were obtained from RIKEN (http://www.brc.riken.jp/lab/epd/Eng/). The entry clones of these genes were constructed by PCR amplication with respectively primers TCH2+attB+F and TCH2+attB+R-stop, CML10+attB+F and CML10+attB+R-stop, CAM2+attB+F and CAM2+attB+R-stop, CML9+attB+F and CML9+attB+R-stop using Phusion High-Fidelity DNA Polymerase (Thermo Scientific). The resulting PCR fragments were recombined into *pDONR207* (BP reaction). All primers used in this study are listed in Table 1. Relevant pDONR sequences of all constructs were checked by sequencing (Macrogen, Amsterdam), and subsequently combined into either pART7- or pET16H-derived destination vectors (LR reaction), containing respectively the YFP- or the His tag coding region in frame with the Gateway cassette (Invitrogen). Gel extraction of PCR products was performed by using the DNA Gel extraction kit from Thermo Scientific.

The PID insertion domain (AA 227 to 280) was exchanged for *Sgs*I and *Bsp*TI restriction sites by amplifying the remaining PID mRNA plus the vector backbone with primer pair ER023/ER024 using *pDONR-PID* as template. This linear PCR product was circularized by ligation of *Bsp*TI restriction site fragments at both termini, yielding *pDONR207-PID –ID*. Fragments of the PID ID were subsequently re-inserted into this construct via the introduced SgsI-BspTI restriction sites. For this purpose DNA fragments coding for the amino acids 227-253, 240-266 and 254-280 of the PID ID with the appropriate restriction site overhangs were generated by annealing oligonucleotides following Sigma-Aldrich's "Protocol for Annealing Oligonucleotides". A 169 bp long DNA fragment, coding for the entire PID ID was obtained by PCR. Following digestion with *Sgs*I and *Bsp*TI and gel purification, this fragment was inserted into the corresponding restriction sites in *pDONR207-PID-ID*. The *pDONR-PID Ala1-3* mutant versions were constructed using the Agilent QuickChange II XL site directed mutagenesis kit, primers ERC064-069, and *pDONR-PID* as template. .

pDONR-PID S/T 250,255A, *pDONR-PID R249,252,253A*, *pDONR-PID R263,266A* were constructed using the Agilent QuickChange II XL site directed mutagenesis kit, primers ER116,117,119, and *pDONR-PID* as template. *pDONR-PID R249,252,253,263,266A* was constructed using Agilent QuickChange II XL site directed mutagenesis kit, primers ER119, and *pDONR-PID R249,252,253A* as template.

The coding regions of M1 to M7 were constructed by PCR amplication using Phusion High-Fidelity DNA Polymerase (Thermo Scientific). The left part of the coding region was PCR amplified with primers PID attB F1 and M1+R+pcr, M2+R+pcr, M3+R+pcr, M4+R+pcr, M5+R+pcr, or M6+R+pcr+9bp using *pDONR-PID* as template. The right part of the coding region was PCR amplified with primers PID attB R1 and M1+F+pcr, M2+F+pcr, M3+F+pcr, M4+F+pcr, M5+F+pcr, or M6+F+pcr also using *pDONR-PID* as template. The complete coding sequences were constructed by PCR amplication using primers PID attB F1 and PID attB R1 and the correct combination of left part and right part PCR products as templates. The resulting PCR fragments were recombined into *pDONR207* (BP reaction, Invitrogen).

All mutant PID versions described above were transferred from the *pDONR* entry vector to expression vectors (*pGEX*, *pET*, *pARF7*) by gateway cloning (LR reaction, Invitrogen).The *pART7:ID:YFP* and *pART7:ID$_{244-275}$:YFP* were constructed by first PCR amplifying a fragment containing the ID or ID244-275 by primers SB001-002 or SB003-004, respectively, adding the restriction sites *Bam*HI and *Hind*III. These products were then cloned into *pART7-YFP-HAII* digested with *Bam*HI and *Hind*III. *pGEX:ID* and *pGEX:ID$_{244-275}$* were constructed by cloning the above digestion products into *pGEX-KG* digested with *Bam*HI and *Hind*III.

Table 1: Primer list

The attB recombination sites are underlined

TCH3 attB F1	5'GGGGACAAGTTTGTACAAAAAAGCAGGCTTAATGGCGGATAAGCTCACT3'
TCH3 attB R1	5'GGGGACCACTTTGTACAAGAAAGCTGGGTAAGATAACAGCGCTTCGAACA3'
PID attB F1	5'GGGGACAAGTTTGTACAAAAAAGCAGGCTTCAGCATGTTACGAGAATCAGAC GGT3'
PID attB R1	5'GGGGACCACTTTGTACAAGAAAGCTGGGTCAAAGTAATCGAACGCCGCTGG3'
PID exon1 F1	5'TCTCTTCCGCCAGGTAAAAA3'
PID exon2 R1	5'CGCAAGACTCGTTGGAAAAG3'
TCH3pr F1	5'AAATGTCCACTCACCCATCC3'

TCH3pr R1	5’GGGAATTCTGAAGATCAGCTTTTGTCG3’
M1+R+pcr:	5’TAAAGTCTGAACCTTTTTAGACCGCTCGTCTCGTTGGAA3’
M1+F+pcr:	5’TTCCAACGAGACGAGCGGTCTAAAAAGGTTCAGACTTTA3’
M2+R+pcr:	5’TAAAGTCTGAACCTCTTCAGACTCCAAGACTCGTTGGAA3’
M2+F+pcr:	5’TTCCAACGAGTCTTGGAGTCTGAAGAGGTTCAGACTTTA3’
PID R1(delete IQ)+M3	5’AGAGACGGGTTGGTTCAAGTCTAGCGAGACGA3’
PID F1(delete IQ)+M3	5’TCGTCTCGCTAGACTTGAACCAACCCGTCTCT3’
PID R2(IQ->A)+M4	5’AGAGACGGGTTGGTTCTCGTCGTCGTCGTCGTCGTCGTCGTCGTCGTCGT CGAAGTCTAGCGAGACGA3’
PID F1(IQ->A)+M4	5’TCGTCTCGCTAGACTTGCTGCTGCTGCTGCTGCTGCTGCTGCTGCTGCTGC TGAACCAACCCGTCTCT3’
M5+R+pcr	5’TAAAGTCTGAACCTCTTCAGACCGCAAGACTCGTTGGAA3’
M5+F+pcr	5’TTCCAACGAGTCTTGCGGTCTGAAGAGGTTCAGACTTTA3’
M6+R+pcr	5’GGTTGGTTCTTCAGTCTGATCCTTTTTAGACCGCAAGACTCGTTGGAA3’
M6+F+pcr	5’TTCCAACGAGTCTTGCGGTCTAAAAAGGATCAGACTGAA3’
CML9+attB+F	5’GGGACAAGTTTGTACAAAAAAGCAGGCTTCATGGCGGATGCTTTCACAGATGAA G3’
CML9+attB+R-stop	5’GGGGACCACTTTGTACAAGAAAGCTGGGTCATAAGAGGCAGCAATCATCA3’
CML10+attB+F	5’GGGGACAAGTTTGTACAAAAAAGCAGGCTTCATGGCGAATAAGTTCACTAG3’
CML10+attB+R-stop	5’GGGGACCACTTTGTACAAGAAAGCTGGGTCAGAAAACAACGCTTCGAACA3’
TCH2+attB+F	5’GGGGACAAGTTTGTACAAAAAAGCAGGCTTCATGTCATCGAAGAACGGAGTTG3’
TCH2+attB+R-stop	5’GGGGACCACTTTGTACAAGAAAGCTGGGTCAGCACCACCACCATTACTCA3’
CAM2+attB+F	5’GGGGACAAGTTTGTACAAAAAAGCAGGCTTCATGGCGGATCAGCTCACAGA3’
CAM2+attB+R-stop	5’GGGGACCACTTTGTACAAGAAAGCTGGGTCCTTAGCCATCATAACCTTCA3’
PID Deletion 2 S (ERC023)	5’AAACTTAAGGGCGCGCCCGAGGTCAAAGTCAGAGAGC3’
PID Deletion 2 AS (ERC024)	5’GACCTTAAGGCTGAACCGGTTACTGC3’
PID InsDom S_1 (ER003)	5’TGGCGCGCCTCTCTATGCTCCGACTCAAT3’
PID InsDom AS_162 (ERC004)	5’CGTCTTAAGAACAAAGAGACGGGTTGG3’
PID InsDom AA227-253 S (ERC005)	5’CGCGCCTCTCTATGCTCCGACTCAATCGCAGCCGTTGAATCTTCCTCGTCTTCG CCGGAGAATCAACAACTCCGTTCACCGCGACGAC3’
PID InsDom AA227-253 AS	5’TTAAGTCGTCGCGGTGAACGGAGTTGTTGATTCTCCGGCGAAGACGAGGAAG

(ERC006)	ATTCAACGGCTGCGATTGAGTCGGAGCATAGAGAGG3’
PID InsDom AA254-280 S (ERC007)	5’CGCGCCTTCACTCGTCTCGCTAGACTTTTCCAACGAGTCTTGCGGTCTAAAAA GGTTCAGACTTTAGAACCAACCCGTCTCTTTGTTC3’
PID InsDom AA254-280 AS (ERC008)	5’TTAAGAACAAAGAGACGGGTTGGTTCTAAAGTCTGAACCTTTTTAGACCGCA AGACTCGTTGGAAAAGTCTAGCGAGACGAGTGAAGG3’
PID InsDom AA240-266 S (ERC009)	5’CGCGCCTCGTCTTCGCCGGAGAATCAACAACTCCGTTCACCGCGACGATTCA CTCGTCTCGCTAGACTTTTCCAACGAGTCTTGCGGC3’
PID InsDom AA240-266 AS (ERC010)	5’TTAAGCCGCAAGACTCGTTGGAAAAGTCTAGCGAGACGAGTGAATCGTCGCG GTGAACGGAGTTGTTGATTCTCCGGCGAAGACGAGG3’
PID-ALA1 S (ERC064)	5’GAATCTTCCTCGTCTTCGCCGGAGAATCAAGCAGCCGCTGCAGCGGCAGCATTC ACTCGTCTCGCTAGACTTTTCCAACG3’
PID-ALA1 AS (ERC065)	5’CGTTGGAAAAGTCTAGCGAGACGAGTGAATGCTGCCGCTGCAGCGGCTGCTTGA TTCTCCGGCGAAGACGAGGAAGATTC3’
PID-ALA2 S (ERC066)	5’GAGAATCAACAACTCCGTTCACCGCGACGAGCCGCTGCTGCCGCTGCAGCTTTC CAACGAGTCTTGCGGTCTAAAAAGGT3’
PID-ALA2 AS (ERC067)	5’ACCTTTTTAGACCGCAAGACTCGTTGGAAAGCTGCAGCGGCAGCAGCGGCTCGT CGCGGTGAACGGAGTTGTTGATTCTC3’
PID-ALA3 S (ERC068)	5’CACCGCGACGATTCACTCGTCTCGCTAGACTTGCCGCAGCAGCCGCGGCGGCTA AAAAGGTTCAGACTTTAGAACCAACCCGT3’
PID-ALA3 AS (ERC069)	5’ACGGGTTGGTTCTAAAGTCTGAACCTTTTTAGCCGCCGCGGCTGCTGCGGCAAGT CTAGCGAGACGAGTGAATCGTCGCGGTG3’
PID InsDom S/T250,255A (ER116)	5’CAACTCCGAGCTCCGCGACGATTCGCTCGTCTCGC3’
PID InsDom R249,252,253A AS (ER117)	5’GTGAATGCTGCAGGTGAAGCGAGTTGTTG 3’
PID InsDom R263,266A (ER119)	5’CTTTTCCAAGCAGTACTGGCGTCTAAAAAGG3’
SB001 attB1 InsDom AA229 S	5’GGGGACAAGTTTGTACAAAAAAGCAGGCTTAATGCTATGCTCCGACTCAATCG3’
SB002 attB2 InsDom AA279 AS	5’GGGGACCACTTTGTACAAGAAAGCTGGGTCAAAGAGACGGGTTGG3’
SB003 attB1 InsDom AA248 S	5’GGGGACAAGTTTGTACAAAAAAGCAGGCTTAATGGAGAATCAACAACTC3’
SB004 attB2 InsDom AA274 AS	5’GGGGACCACTTTGTACAAGAAAGCTGGGTGTTCTAAAGTCTGAACC3’

In vitro pull-down

In vitro pull-down analysis was performed as previously described (Benjamins et al.,

2003).

Protoplast transfection and Förster (Fluorescence) Resonance Energy Transfer (FRET) analysis

Protoplasts were obtained from *Arabidopsis thaliana* Col-0 cell suspension cultures that were propagated as described (Schirawski et al., 2000). Protoplast isolation and PEG-mediated transfections with 10 µg plasmid DNA were performed as adapted by Schirawski and coworkers (Schirawski et al., 2000). To obtain auxin-starved protoplasts, auxin (NAA) was removed from the media during protoplast isolation. Following transfection, the protoplasts were incubated for at least 16 hours in the dark prior to observation.

All microscopic analyses were done with a Zeiss LSM5 Exciter (Zeiss, Oberkochen, Germany) using a 63x magnifying objective. The CFP signal was detected using an argon 458 nm laser and a 475-525 nm band pass filter. The YFP signal was detected using an argon 514 nm laser and a 530-600 nm band pass filter. To detect FRET, a 458 nm laser and a 530 nm long pass filter were used, and images were anlysed with a sensitized emission FRET approach by using the Image J plugin *FRET and Colocalization Analyzer*. This plugin allows calculation of a FRET index on a pixel by pixel basis and corrects for donor bleed through, acceptor bleed through and false FRET (by associating FRET with colocalization of the two fluorophores). "Donor only" protoplasts expressing *35S::CFP* and "acceptor only" protoplasts expressing *35S::YFP* were used to determine donor bleed through and acceptor bleed through, respectively. Protoplasts transfected with the *35S::CFP-YFP* construct were used as positive control. The Image J plugin calculated the FRET index. The relative FRET image was obtained by dividing the FRET index by the YFP channel image. For each protoplast three fixed areas (regions of interest, ROIs) were quantified using the ImageJ software. Per sample scanning was performed on ten protoplasts. The obtained intensities of all protoplasts were averaged and used to calculate the standard deviation. The Student's *t*-test was used to test for significant differences in relative FRET ($p<0.05$ level).

Protein alignment, phylogenetic tree, and helix wheel projection

The PID ID structure was predicted by both http://zhanglab.ccmb.med.umich.edu/QUARK/ and http://bioserv.rpbs.univ-paris-diderot.fr/PEP-FOLD/. Based on the characterization of multiple IQ motifs the following consensus was established for IQ-

([FILV]Qxxx[RK]Gxxx[RK]xx[FILVWY]) or IQ-like motifs ([FILV]Qxxx[RK]xxxxxxxxx). The amino acid residues between brackets can substitute for each other at that specific position (http://calcium.uhnres.utoronto.ca/ctdb/ctdb/motifs/iq_motif.html). The helix wheel projection was made by http://heliquest.ipmc.cnrs.fr/.

All calmodulin protein sequences were downloaded from TAIR (http://www.arabidopsis.org/). The phylogenetic tree and calmodulin alignment were constructed with the CLC Main Workbench 6.9.1 software (CLC Bio/Qiagen).

Accession Numbers

The *Arabidopsis* Genome Initiative locus identifiers for the genes mentioned are as follows: *PID* (At2g34650, pda07777), WAG2 (At3g14370), TCH3 (At2g41100, pda09314), TCH2 (AT5g37770, pda17915), CML10(AT2g41090, pda01448), CAM2 (At2g41110, pda02964), CML9 (Atg51920, pda00144).

Acknowledgements

The project was supported by a TOP grant from the Research Council for Chemical Sciences (700.58.301) to R.O., with financial aid from the Netherlands Organization of Scientific Research (NWO). The authors would like to thank Gerda Lamers, Ward de Winter and Jan Vink for their help with the microscopy, tissue culture and plant caretaking, respectively.

Reference

Abas, L., Benjamins, R., Malenica, N., Paciorek, T., Wisniewska, J., Moulinier-Anzola, J.C., Sieberer, T., Friml, J., and Luschnig, C. (2006). Intracellular trafficking and proteolysis of the *Arabidopsis* auxin-efflux facilitator PIN2 are involved in root gravitropism. Nat Cell Biol **8,** 249-256.

Bahler, M., and Rhoads, A. (2002). Calmodulin signaling via the IQ motif. FEBS Lett **513,** 107-113.

Benjamins, R., Ampudia, C.S., Hooykaas, P.J., and Offringa, R. (2003). PINOID-mediated signaling involves calcium-binding proteins. Plant Physiol **132,** 1623-1630.

Bhardwaj, R., Muller, H.M., Nickel, W., and Seedorf, M. (2013). Oligomerization and Ca^{2+}/calmodulin control binding of the ER Ca^{2+}-sensors STIM1 and STIM2 to

plasma membrane lipids. Biosci Rep **33**.

Braam, J., and Davis, R.W. (1990). Rain-, wind-, and touch-induced expression of calmodulin and calmodulin-related genes in Arabidopsis. Cell **60,** 357-364.

Chin, D., and Means, A.R. (2000). Calmodulin: a prototypical calcium sensor. Trends Cell Biol **10,** 322-328.

Clapham, D.E. (2007). Calcium signaling. Cell **131,** 1047-1058.

Cornell, R.B., and Taneva, S.G. (2006). Amphipathic helices as mediators of the membrane interaction of amphitropic proteins, and as modulators of bilayer physical properties. Curr Protein Pept Sci **7,** 539-552.

Dhonukshe, P., Huang, F., Galvan-Ampudia, C.S., Mahonen, A.P., Kleine-Vehn, J., Xu, J., Quint, A., Prasad, K., Friml, J., Scheres, B., and Offringa, R. (2010). Plasma membrane-bound AGC3 kinases phosphorylate PIN auxin carriers at TPRXS(N/S) motifs to direct apical PIN recycling. Development **137,** 3245-3255.

Ding, Z., Galvan-Ampudia, C.S., Demarsy, E., Langowski, L., Kleine-Vehn, J., Fan, Y., Morita, M.T., Tasaka, M., Fankhauser, C., Offringa, R., and Friml, J. (2011). Light-mediated polarization of the PIN3 auxin transporter for the phototropic response in *Arabidopsis*. Nat Cell Biol **13,** 447-452.

Du, L., and Poovaiah, B.W. (2005). Ca^{2+}/calmodulin is critical for brassinosteroid biosynthesis and plant growth. Nature **437,** 741-745.

Du, L., Ali, G.S., Simons, K.A., Hou, J., Yang, T., Reddy, A.S., and Poovaiah, B.W. (2009). Ca^{2+}/calmodulin regulates salicylic-acid-mediated plant immunity. Nature **457,** 1154-1158.

Friml, J., Yang, X., Michniewicz, M., Weijers, D., Quint, A., Tietz, O., Benjamins, R., Ouwerkerk, P.B., Ljung, K., Sandberg, G., Hooykaas, P.J., Palme, K., and Offringa, R. (2004). A PINOID-dependent binary switch in apical-basal PIN polar targeting directs auxin efflux. Science **306,** 862-865.

Galván-Ampudia, C.S., and Offringa, R. (2007). Plant evolution: AGC kinases tell the auxin tale. Trends Plant Sci. **12,** 541-547.

Geldner, N., Friml, J., Stierhof, Y.D., Jurgens, G., and Palme, K. (2001). Auxin transport inhibitors block PIN1 cycling and vesicle trafficking. Nature **413,** 425-428.

Heximer, S.P., Lim, H., Bernard, J.L., and Blumer, K.J. (2001). Mechanisms governing subcellular localization and function of human RGS2. J Biol Chem **276,** 14195-14203.

Hoeflich, K.P., and Ikura, M. (2002). Calmodulin in action: diversity in target

recognition and activation mechanisms. Cell **108,** 739-742.

Houdusse, A., and Cohen, C. (1995). Target sequence recognition by the calmodulin superfamily: implications from light chain binding to the regulatory domain of scallop myosin. Proc Natl Acad Sci U S A **92,** 10644-10647.

Houdusse, A., Gaucher, J.F., Krementsova, E., Mui, S., Trybus, K.M., and Cohen, C. (2006). Crystal structure of apo-calmodulin bound to the first two IQ motifs of myosin V reveals essential recognition features. Proc Natl Acad Sci U S A **103,** 19326-19331.

Huang, F., Zago, M.K., Abas, L., van Marion, A., Galvan-Ampudia, C.S., and Offringa, R. (2010). Phosphorylation of conserved PIN motifs directs *Arabidopsis* PIN1 polarity and auxin transport. Plant Cell **22,** 1129-1142.

Knight, H. (2000). Calcium signaling during abiotic stress in plants. Int Rev Cytol **195,** 269-324.

Knight, M.R., Campbell, A.K., Smith, S.M., and Trewavas, A.J. (1991). Transgenic plant aequorin reports the effects of touch and cold-shock and elicitors on cytoplasmic calcium. Nature **352,** 524-526.

Lu, F., and Taghbalout, A. (2013). Membrane association via an amino-terminal amphipathic helix is required for the cellular organization and function of RNase II. J Biol Chem **288,** 7241-7251.

McCormack, E., and Braam, J. (2003). Calmodulins and related potential calcium sensors of Arabidopsis. New Phytol. **159,** 585-598.

McCormack, E., Tsai, Y.-C., and Braam, J. (2005). Handling calcium signaling: Arabidopsis CaMs and CMLs. Trends in Plant Science **10,** 383-389.

McLaughlin, S., and Murray, D. (2005). Plasma membrane phosphoinositide organization by protein electrostatics. Nature **438,** 605-611.

Monshausen, G.B., Bibikova, T.N., Weisenseel, M.H., and Gilroy, S. (2009). Ca^{2+} regulates reactive oxygen species production and pH during mechanosensing in *Arabidopsis* roots. Plant Cell **21,** 2341-2356.

Monshausen, G.B., Miller, N.D., Murphy, A.S., and Gilroy, S. (2011). Dynamics of auxin-dependent Ca^{2+} and pH signaling in root growth revealed by integrating high-resolution imaging with automated computer vision-based analysis. Plant J. **65,** 309-318.

Munshi, H.G., Burks, D.J., Joyal, J.L., White, M.F., and Sacks, D.B. (1996). Ca^{2+} regulates calmodulin binding to IQ motifs in IRS-1. Biochemistry **35,** 15883-15889.

Olivotto, M., Arcangeli, A., Carla, M., and Wanke, E. (1996). Electric fields at the plasma membrane level: a neglected element in the mechanisms of cell signalling. Bioessays **18,** 495-504.

Petrasek, J., Mravec, J., Bouchard, R., Blakeslee, J.J., Abas, M., Seifertova, D., Wisniewska, J., Tadele, Z., Kubes, M., Covanova, M., Dhonukshe, P., Skupa, P., Benkova, E., Perry, L., Krecek, P., Lee, O.R., Fink, G.R., Geisler, M., Murphy, A.S., Luschnig, C., Zazimalova, E., and Friml, J. (2006). PIN proteins perform a rate-limiting function in cellular auxin efflux. Science **312,** 914-918.

Polisensky, D.H., and Braam, J. (1996). Cold-shock regulation of the Arabidopsis TCH genes and the effects of modulating intracellular calcium levels. Plant Physiol **111,** 1271-1279.

Poovaiah, B.W., Du, L., Wang, H., and Yang, T. (2013). Recent advances in calcium/calmodulin-mediated signaling with an emphasis on plant-microbe interactions. Plant Physiol **163,** 531-542.

Popescu, S.C., Popescu, G.V., Bachan, S., Zhang, Z., Seay, M., Gerstein, M., Snyder, M., and Dinesh-Kumar, S.P. (2007). Differential binding of calmodulin-related proteins to their targets revealed through high-density *Arabidopsis* protein microarrays. Proc Natl Acad Sci U S A **104,** 4730-4735.

Rademacher, E.H., and Offringa, R. (2012). Evolutionary adaptations of plant AGC Kinases: from light signaling to cell polarity regulation. Front Plant Sci **3,** 250.

Rhoads, A.R., and Friedberg, F. (1997). Sequence motifs for calmodulin recognition. FASEB J **11,** 331-340.

Roberts, D.M., and Harmon, A.C. (1992). Calcium-modulated proteins: targets of intracellular calcium signals in higher plants. Annu. Rev. Plant Physiol. Plant Mol. Biol. **43,** 375-414.

Sambrook, J., Fritsch F. and Maniatis, T. (1989). Molecular cloning-A laboratory mannual. Cold Spring Harbor Laboratory press, NY, USA.

Sauer, M., Balla, J., Luschnig, C., Wisniewska, J., Reinohl, V., Friml, J., and Benkova, E. (2006). Canalization of auxin flow by Aux/IAA-ARF-dependent feedback regulation of PIN polarity. Genes Dev **20,** 2902-2911.

Schirawski, J., Planchais, S., and Haenni, A.L. (2000). An improved protocol for the preparation of protoplasts from an established *Arabidopsis thaliana* cell suspension culture and infection with RNA of turnip yellow mosaic tymovirus: a simple and reliable method. J Virol Methods **86,** 85-94.

Snedden, W.A., and Fromm, H. (2001). Calmodulin as a versatile calcium signal transducer in plants. New Phytol **151,** 35-66.

Stahelin, R.V., Scott, J.L., and Frick, C.T. (2014). Cellular and molecular interactions of phosphoinositides and peripheral proteins. Chem Phys Lipids.

Tanaka, H., Dhonukshe, P., Brewer, P.B., and Friml, J. (2006). Spatiotemporal asymmetric auxin distribution: a means to coordinate plant development. Cell Mol Life Sci **63,** 2738-2754.

Trewavas, A.J., and Malho, R. (1998). Ca^{2+} signalling in plant cells: the big network! Curr Opin Plant Biol **1,** 428-433.

Wisniewska, J., Xu, J., Seifertova, D., Brewer, P.B., Ruzicka, K., Blilou, I., Rouquie, D., Benkova, E., Scheres, B., and Friml, J. (2006). Polar PIN localization directs auxin flow in plants. Science **312,** 883.

Xie, X., Harrison, D.H., Schlichting, I., Sweet, R.M., Kalabokis, V.N., Szent-Gyorgyi, A.G., and Cohen, C. (1994). Structure of the regulatory domain of scallop myosin at 2.8 A resolution. Nature **368,** 306-312.

Yap, K., Kim, J., Truong, K., Sherman, M., Yuan, T., and Ikura, M. (2000). Calmodulin target database. J Struct and Funct Genomics **1,** 8-14.

Zegzouti, H., Anthony, R.G., Jahchan, N., Bogre, L., and Christensen, S.K. (2006a). Phosphorylation and activation of PINOID by the phospholipid signaling kinase 3-phosphoinositide-dependent protein kinase 1 (PDK1) in *Arabidopsis*. Proc Natl Acad Sci U S A **103,** 6404-6409.

Zegzouti, H., Li, W., Lorenz, T.C., Xie, M., Payne, C.T., Smith, K., Glenny, S., Payne, G.S., and Christensen, S.K. (2006b). Structural and functional insights into the regulation of *Arabidopsis* AGC VIIIa kinases. J Biol Chem **281,** 35520-35530.

Zielinski, R.E. (1998). Calmodulin and calmodulin-binding proteins in plants. Annu Rev Plant Physiol Plant Mol Biol **49,** 697-725.